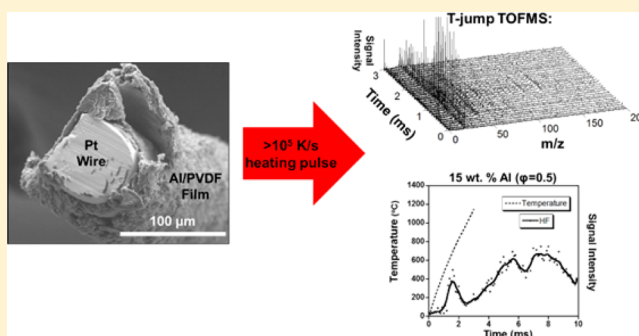


# Probing the Reaction Mechanism of Aluminum/Poly(vinylidene fluoride) Composites

Jeffery B. DeLisio,<sup>†</sup> Xiuli Hu,<sup>†</sup> Tao Wu,<sup>†</sup> Garth C. Egan,<sup>†</sup> Gregory Young,<sup>‡</sup> and Michael R. Zachariah<sup>\*,†</sup><sup>†</sup>Department of Chemistry and Biochemistry and Department of Chemical and Biomolecular Engineering, University of Maryland, College Park, Maryland 20742, United States<sup>‡</sup>Naval Surface Warfare Center – Indian Head Division, Indian Head, Maryland 20640, United States

## S Supporting Information

**ABSTRACT:** Energetic thin films with high mass loadings of nanosized components have been recently fabricated using electrospray deposition. These films are composed of aluminum nanoparticles (nAl) homogeneously dispersed in an energetic fluoropolymer binder, poly(vinylidene fluoride) (PVDF). The nascent oxide shell of the nAl has been previously shown to undergo a preignition reaction (PIR) with fluoropolymers such as polytetrafluoroethylene (PTFE). This work examines the PIR between alumina and PVDF to further explain the reaction mechanism of the Al/PVDF system. Temperature jump (T-jump) ignition experiments in air, argon, and vacuum environments showed that the nAl is fluorinated by gas phase species due to a decrease in reactivity in a vacuum. Thermogravimetric analysis coupled with differential scanning calorimetry (TGA/DSC) was used to confirm the occurrence of a PIR, and gas phase products during the PIR and fluorination of nAl were investigated with temperature jump time-of-flight mass spectrometry (T-jump TOFMS). Results show a direct correlation between the amount of alumina in the PVDF film and the relative signal intensity of hydrogen fluoride release (HF). Although the PIR between alumina and PVDF plays an important role in the Al/PVDF reaction mechanism, burn speeds of Al/PVDF films containing additional pure alumina particles showed no burn speed enhancement.



## INTRODUCTION

Aluminum particles have been extensively employed as a fuel in solid rocket propellants due to aluminum's desirable combustion characteristics.<sup>1</sup> Nanosized aluminum (nAl) particles are now readily available and have been implemented into various energetic formulations.<sup>2</sup> The primary motivation for nanosized components is decreased diffusion lengths and an increase in the mass specific burning rate. In typical propellant applications, a binder must be employed to give the propellant mechanical integrity and ideally to enhance the combustion properties of the system.<sup>3</sup> Fluoropolymer binders are one type of energetic binder, which favorably reacts with the aluminum fuel to create aluminum fluoride (AlF<sub>3</sub>).

Polytetrafluoroethylene (PTFE), also known as Teflon, has been extensively used for the fluorination of aluminum in energetic formulations due to the high density of fluorine atoms within the polymer.<sup>4,5</sup> The Al/PTFE reaction mechanism has previously been studied, and a preignition reaction (PIR) has been observed that is proposed to play an important role in the reaction mechanism between Al and a fluoropolymer.<sup>6</sup> The PIR is proposed to arise from the fluorination of the native Al<sub>2</sub>O<sub>3</sub> passivation shell on aluminum particles.<sup>7</sup> With most aluminum nanopowders being between ~70–80% active, there is a significant weight percent of alumina in these composites that can contribute to this reaction. As nAl particle size decreases,

the amount of Al<sub>2</sub>O<sub>3</sub> in the particle on a per mass basis is increased resulting in an enhanced PIR leading to increased ignition sensitivity and exothermicity.<sup>6</sup>

Although PTFE has one of the highest fluorine concentrations among the commonly used fluoropolymers, it poses many processing issues because PTFE is insoluble in most solvents. However, poly(vinylidene fluoride) (PVDF) does not have these solubility issues and has recently been employed as an energetic binder for nAl<sup>8</sup> using an additive manufacturing approach. In this approach, electrospray deposition was employed to avoid the difficulties in mixing nanoparticles in polymer systems and thus enabling the fabrication of high metal loaded polymer.<sup>8,9</sup> This approach also enables the fabrication of graded or laminate structures with different mechanical and combustion performance. These properties make Al/PVDF highly desirable for a wide range of potential applications, but composites involving nAl have not yet been widely studied and more information is needed on the fluorination mechanism.

Of particular interest is the PIR that has been observed in the Al/PTFE system as well as multiple other systems employing halogen-containing oxidizers such as the Al/perfluoropolyether

Received: February 1, 2016

Revised: May 25, 2016

Published: May 26, 2016

(PFPE) and Al/I<sub>2</sub>O<sub>5</sub> systems.<sup>10,11</sup> Preliminary work by our group has proposed that a similar PIR occurs in the Al/PVDF system as well.<sup>8</sup> However, the exact role or importance of the PIR in the combustion Al/PVDF has not yet been fully explored. Here, we will investigate this process in the context of the broader mechanisms of reaction and propagation. In particular, we focus on using techniques that allow for exploring a wide range of heating rates, including those that are representative of free combustion.

Previous works have used standard differential scanning calorimetry (DSC) and thermogravimetric analysis (TGA) techniques to investigate the Al/PTFE PIR and a direct correlation between exothermicity of the PIR and heating rate has been observed.<sup>12</sup> However, the highest heating rate tested in that work was 780 °C/min. In comparison, the temperature jump (T-jump) ignition experiments can increase the heating rate of the material to ~10<sup>5</sup> °C/s, which can more realistically represent a combustion event.<sup>13</sup> Ignition experiments using the T-jump technique were performed in different environments and pressures to probe the effect of the surrounding gases on the overall Al/PVDF reaction mechanism. Since little information on the species created before and during ignition has been obtained, we employ T-jump ignition coupled to time-of-flight mass spectrometry (TOFMS) to investigate the role of the PIR in the overall reaction mechanism at much shorter time scales.

In this work, the PIR between Al<sub>2</sub>O<sub>3</sub> and PVDF is explored to determine its role in the reaction mechanism between nAl and PVDF. PIRs have been studied in other halogen-containing systems but have yet to be fully investigated in the Al/PVDF system.<sup>6,7,10,11,14</sup> We examine the exact nature of how nAl is fluorinated in an energetic thin film employing PVDF as an energetic binder. Further understanding of this mechanism may allow for the creation of tailored energetic laminates and multicomponent nanocomposites. Gas phase decomposition products of fluoropolymers exhibiting PIRs with Al<sub>2</sub>O<sub>3</sub> have yet to be analyzed on time scales representative of combustion, which will be the main focus of this work. Results show that nAl is fluorinated by gas phase decomposition products from the PVDF, and the nature of the PVDF decomposition is directly correlated to the amount of Al<sub>2</sub>O<sub>3</sub> in the film. These new findings are then used to determine if altering the decomposition of PVDF by adding Al<sub>2</sub>O<sub>3</sub> can affect the burn speed of thin films.

## ■ EXPERIMENTAL SECTION

**Materials.** The nAl used in this work were purchased from Novacentrix with an active Al content of 81 mass %, determined by thermogravimetric analysis (TGA). The Al<sub>2</sub>O<sub>3</sub> nanopowder (<50 nm), poly(vinylidene fluoride) (PVDF) (MW = 534 000), and dimethylformamide (DMF) (99.8 wt %) were purchased from Sigma-Aldrich.

**Precursor Preparation and Film Deposition.** Al/PVDF thin films were created using the previously described electro-spray-based deposition method.<sup>8</sup> This method allows for the creation of films with high mass loadings while avoiding the increased viscosity issues associated with traditional nanopowder-containing polymer melts. Al/PVDF films of 50 wt % Al were synthesized for the initial T-jump ignition tests. Al/PVDF equivalence ratios of 0.5, 1, and 2 were synthesized for T-jump TOFMS experiments probing the release of gas phase species, which correspond to Al mass loadings of 15, 25, and 40 wt %. The equivalence ratio in this work corresponds to

the Al to F ratio to give the main reaction product, AlF<sub>3</sub>. Al<sub>2</sub>O<sub>3</sub>/PVDF films were also made with the same Al<sub>2</sub>O<sub>3</sub>:PVDF mass loadings as the Al/PVDF films in order to further probe the PIR. Films prepared for burn speed tests used a stoichiometric ratio of Al:PVDF (25 wt % Al) with varying amounts of 50 nm Al<sub>2</sub>O<sub>3</sub> added to the precursor solution before sonication/stirring. Precursor solutions for the films prepared for burn speed tests used 8 mL of DMF with a 50 mg/mL loading of PVDF in addition to the varying amounts of Al and Al<sub>2</sub>O<sub>3</sub>. A distance of 4 cm and voltage differential of 18 kV between the electro-spray needle and the collection substrate were employed as the parameters for electro-spray deposition. The electro-spray setup was also modified to coat a thin platinum (Pt) wire (76 μm diameter), approximately 10 mm in length with a 3–5 mm length of coating, to be used for the T-jump experiments. When depositing films onto the Pt wire, a deposition time of 15 min at a rate of 2 mL/h was used, resulting in an ~5 μm thick film on the wire. Free-standing film thicknesses ranged from 50 to 100 μm.

**Characterization.** Ignition temperature tests were performed using T-jump heating of a platinum wire (76 μm diameter) coated with an electro-sprayed Al/PVDF film approximately 3–5 mm in length inside of a chamber pressurized to a specified value. The Callendar–Van Dusen equation was used to correlate the resistance of the wire to a time-resolved temperature by recording the voltage across, and current through the wire during heating, with a 600 MHz digital oscilloscope.<sup>13</sup> The platinum wire was heated with a heating rate of approximately 5 × 10<sup>5</sup> K/s in these experiments for approximately 3 ms. High-speed video was taken using a Phantom v12.0 digital camera running Phantom 692 software. The videos were recorded at 67 000 frames/s. Ignition time and temperature were then determined from the recordings and T-jump data.

Thermogravimetric (TG) and differential scanning calorimetry (DSC) experiments were performed on a SDT Q600 (TA Instruments) under 100 mL/min of O<sub>2</sub> flow. 1–2 mg samples were placed into an alumina pan and heated from room temperature up to 1000 °C at a rate of 5–50 °C/min. No discernible difference in TGA/DSC results were observed between stock PVDF powders and electro-sprayed PVDF films.

Temperature jump time-of-flight mass spectrometry (T-jump TOFMS) was performed using a previously described home-built instrument.<sup>13</sup> Samples were electro-sprayed onto a 76 μm diameter platinum wire for use in the TOFMS and for ignition temperature tests. The same heating parameters and wire temperature calculations were performed as in the T-jump ignition experiments described above. A sampling rate of 100 μs per spectrum (10 kHz) was used to capture the progress of the reaction with 100 spectra obtained post-triggering for each run. The data were captured using a 600 MHz digital oscilloscope.

PVDF films and Al<sub>2</sub>O<sub>3</sub>/PVDF films (before and after heating) were analyzed using X-ray diffraction (XRD; Bruker C2 Discover with GADDS, operating at 40 kV and 40 mA with unfiltered Cu Kα radiation, E 1/4 8049 eV, k 1/4 1.5406 Å).

Burn speed tests were performed in accordance with the parameters previously described in similar work on energetic thin films.<sup>8,9</sup> Strips of each film (0.5 cm × 3.0 cm × ~0.01 cm) were ignited using a resistively heated nichrome wire in a small chamber purged with argon for 15 min. High speed video was taken of the flame propagation, using a Phantom Miro M110 recording at 7000 fps with an exposure of 40 μs, in order to calculate a burn speed for each film.

## RESULTS AND DISCUSSION

**T-Jump Ignition.** In order to evaluate the reactivity of the Al/PVDF films, precursor solutions were directly electro-sprayed onto platinum T-jump filaments using the electro-spray deposition setup shown in Figure 1A.

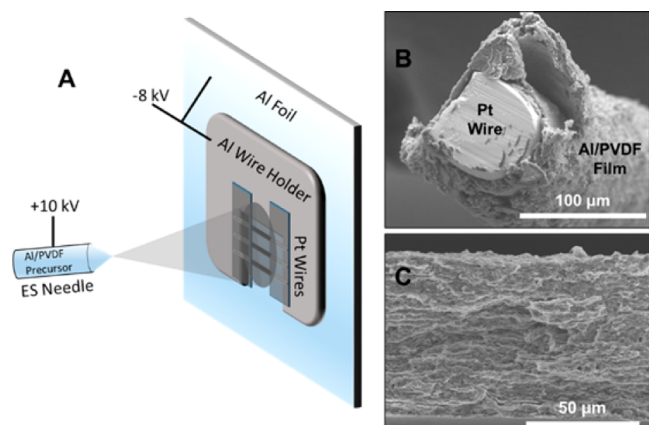


**Figure 1.** Pt wire electro-spray deposition setup (A), cross section of coated Pt wire (B), and cross section of 20 wt % Al/PVDF free-standing film (C).

A 50 mass % Al/PVDF ratio was found to be the highest nAl loading that enabled a crack-free, mechanically flexible film; therefore, this ratio was used for preliminary T-jump ignition tests.<sup>8</sup> T-jump ignition experiments were run in air, argon, and vacuum environments and show a decrease in reactivity between air and argon and negligible reactivity in vacuum (Figure S1). The increased reactivity of samples ignited in air can be attributed to the participation of  $O_{2(g)}$  in the oxidation of the Al as well as production of oxygenated carbon. The significant decrease in reactivity at low pressures suggests that gas phase reaction products must also be participating in the overall reaction. Zulfiquar et al. have reported that the main decomposition product of PVDF is hydrogen fluoride (HF).<sup>15</sup> These results suggest that the Al/PVDF reaction is a two-step process where the PVDF must first decompose into HF, which then enables the fluorination of the Al. The exact composition of these gas phase decomposition species at time scales relevant to reaction will be further analyzed using other techniques later in this paper.

In order to further explore how Al is being oxidized by a gas phase product from the decomposition of PVDF, T-jump experiments were performed to measure the ignition temperature ( $T_{ign}$ ) in air and argon at pressures of 0.1 to ~9 MPa. Figure 2 shows a decrease in ignition temperature of over 250 °C as the pressure is increased, consistent with Al reaction with a gaseous reaction product that has constrained diffusion at higher pressures. The higher ignition temperature at 1 atm of argon, when compared to 1 atm of air, implies that reaction is initiated by gas phase oxygen at this pressure, while at elevated pressures, there is no discernible difference in ignition temperature between argon and oxygen environments, suggesting that ignition is initiated by the PVDF decomposition products at these pressures.

**Slow Heating Chemistry by TGA/DSC.** As mentioned above, slow heating rate TGA/DSC in argon environments has been frequently used to investigate the reaction mechanism between aluminum and fluoropolymers.<sup>8</sup> Previous TGA results

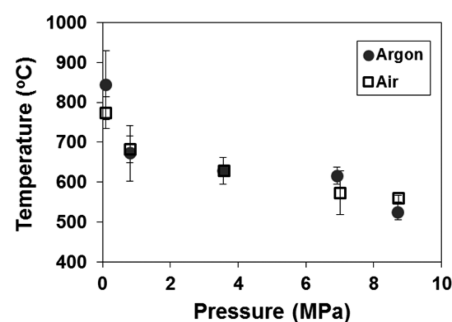


**Figure 2.** Ignition temperature vs pressure for Al/PVDF film electro-sprayed onto a platinum wire in air and argon.

at 20 °C/min shown by our group indicate that pure PVDF films lose the majority of their mass, corresponding to decomposition, at 500 °C while Al/PVDF films show the majority of their mass loss ~100 °C lower at a temperature of 400 °C.<sup>8</sup> Previous work by Pantoya et al. has shown that the alumina shell of nano- to micron-sized aluminum particles can react with fluoropolymers, such as PTFE and PFPE, before ignition in what is referred to as the preignition reaction (PIR).<sup>7,14</sup> In previous work, we state that the first mass loss seen (between 190 and 300 °C) in the TGA of Al/PVDF films corresponds to the PIR between the  $Al_2O_3$  shell of the nAl and the PVDF. Figure S2 highlights the initial mass loss and PIR seen in TGA/DSC results for an  $Al_2O_3$ /PVDF film heated under 100 mL/min of argon flow.

In this work, a slightly different approach was taken to tweeze out the effect of  $Al_2O_3$  on the decomposition of PVDF as compared to prior work.<sup>6,8,12</sup> When standard DSC experiments are run in argon, the PIR exotherm in  $Al_2O_3$ /fluoropolymer systems can potentially be hidden by the large PVDF decomposition endotherm immediately following the PIR. In addition, the fluorine containing decomposition products can react with the alumina pan used in the TGA/DSC complicating the results (Figure S3). In order to further investigate the  $Al_2O_3$ /PVDF PIR and its effect on PVDF decomposition, TGA/DSC of pure PVDF and  $Al_2O_3$ /PVDF films (40 wt %  $Al_2O_3$ ) were run under 100 mL/min of pure  $O_2$ . Further, since Hobosyan et al. demonstrated that heating rate plays an important role in the exothermicity of the PIR,<sup>12</sup> we employed 5, 20, and 50 °C/min heating ramps. It is important to note that the combustion of PVDF in  $O_2$  will be an exothermic process with an onset temperature close to the decomposition temperature of PVDF under the respective heating conditions.

Figure 3 shows TGA and DSC results for the reaction of PVDF and  $Al_2O_3$ /PVDF films with oxygen at heating rates of 5, 20, and 50 °C/min. Figure 3A shows two stages of mass loss when the PVDF film is heated in  $O_2$  with onset temperatures increasing with an increase in heating rate. Two exotherms, due to the oxidation of PVDF decomposition products, are observed in Figure 3C that correspond to these mass loss events with the distinction between the two peaks becoming less apparent with an increase in heating rate.

When compared to previous PVDF decomposition analysis by our group in argon at 20 °C/min, the 20 °C/min run in  $O_2$  has a similar onset temperature of ~440 °C.<sup>8</sup> It can be inferred from this comparison that the PVDF decomposes at the same temperature with and without the presence of  $O_2$ . Previous work also showed a final wt %, when heated in argon, of ~20–25 wt % that corresponds to remaining carbon from PVDF.<sup>8</sup> PVDF is composed of 37.5 wt % carbon; therefore, carbon-

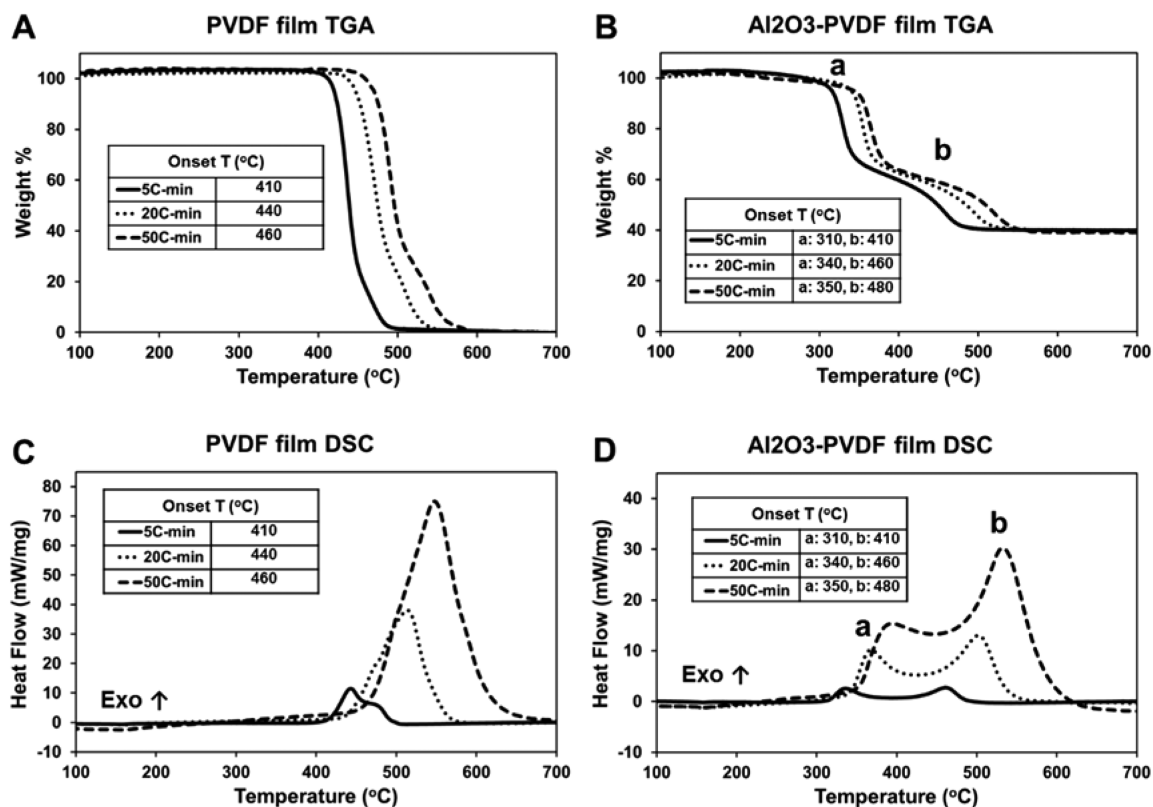


**Figure 3.** TGA/DSC data with labeled respective peak onset temperatures at heating rates of 5, 20, and 50 °C/min under 100 mL/min O<sub>2</sub> flow of PVDF and Al<sub>2</sub>O<sub>3</sub>/PVDF films containing 40 wt % Al<sub>2</sub>O<sub>3</sub>.

containing gas phase decomposition products must be formed to attribute for this discrepancy. In Figure 3A, the second stage of mass loss, which begins at ~25 wt %, can be attributed to the oxidation of this residual carbon due to the presence of oxygen in the system.

It is also important to note that the heat release from the oxidation of carbon increases with increasing heating rate. Previous work investigating the burn rates of Al/PVDF films showed a faster burn rate in an oxygen-containing atmosphere.<sup>8</sup> This was explained by the added oxidation of the nAl by atmospheric oxygen.<sup>8</sup> The TGA/DSC data in Figure 3 further supports a faster burn speed in air as it indicates that oxygen plays an important role in oxidizing the PVDF, which has an increased heat release at higher heating rates.

When Al<sub>2</sub>O<sub>3</sub> is incorporated into PVDF films, two main mass losses are also observed (Figure 3B) corresponding to two distinct exotherms (Figure 3D), the first of which occurs at a much lower temperature than in the pure PVDF. The decrease in onset temperature is 100–110 °C, depending on the heating rate employed. This decrease in decomposition temperature of PVDF can be attributed to the PIR between Al<sub>2</sub>O<sub>3</sub> and the condensed phase fluorine of the PVDF as has been previously seen in other Al/fluoropolymer systems such as Al/PTFE.<sup>6</sup> The PIR occurs prior to the first large exotherm in Figure 3D and initiates the lower temperature decomposition/oxidation of the PVDF. We observe an increase in our first exotherm in Figure 3D with an increase in heating rate similar to Al/PTFE.<sup>12</sup> There is also no significant mass loss before the PIR occurs, signifying that the Al<sub>2</sub>O<sub>3</sub> reacts with PVDF through the condensed phase to catalyze the fluoropolymer's decomposition similar to Al/PTFE.<sup>6</sup> The second main mass loss, with an onset temperature between 400 and 500 °C in Figure 3B, occurs at the same

temperature as pure PVDF. This mass loss can again be attributed to the oxidation of residual condensed phase carbon-containing species left behind from the decomposition of PVDF. This step is unaffected by the presence of Al<sub>2</sub>O<sub>3</sub> in the film, as it occurs at the same temperature with and without Al<sub>2</sub>O<sub>3</sub>. Figure 3B shows a final mass of ~40 wt % corresponding to the 40 wt % Al<sub>2</sub>O<sub>3</sub> in the film. The remaining Al<sub>2</sub>O<sub>3</sub> was later analyzed using XRD to see the extent of any fluorination of the Al<sub>2</sub>O<sub>3</sub>.

The PIR in the Al/PTFE system has been explained by Osborne et al. to be of significance to the oxidation of nAl mainly because of the fluorination of the Al<sub>2</sub>O<sub>3</sub> shell exposing the Al core to allow for enhanced reaction kinetics.<sup>6</sup> The PIR of the Al<sub>2</sub>O<sub>3</sub>/PVDF system precedes the first main mass loss in the TGA similar to what has been observed in other Al/fluoropolymer systems.<sup>6</sup> As discussed in the T-jump ignition experiments, the nAl in the Al/PVDF system is oxidized by gas phase reactants. In addition to the potential exposure of the Al core after the PIR, the observed lower temperature exothermic mass loss seen in Figure 3B,C could play an additional important role in the reaction mechanism by releasing oxidative gas phase species more rapidly at a lower temperature. The first mass loss in Figure 3B, which correlates to the release of fluorine-containing gas phase species facilitated by the condensed phase reaction between PVDF and Al<sub>2</sub>O<sub>3</sub>, was also shown in Figure 3D to be increasingly exothermic with an increase in heating rate supporting the need for a high heating rate analysis of the exact nature of this decomposition.

**Fast-Heating Chemistry by T-Jump TOFMS.** We begin with the mass spectrum of pure PVDF film electrospray onto a Pt wire at a snapshot in time (1.6 ms at a heating rate of ~4 × 10<sup>5</sup> K/s) to show predominant species in Figure 4. T-jump

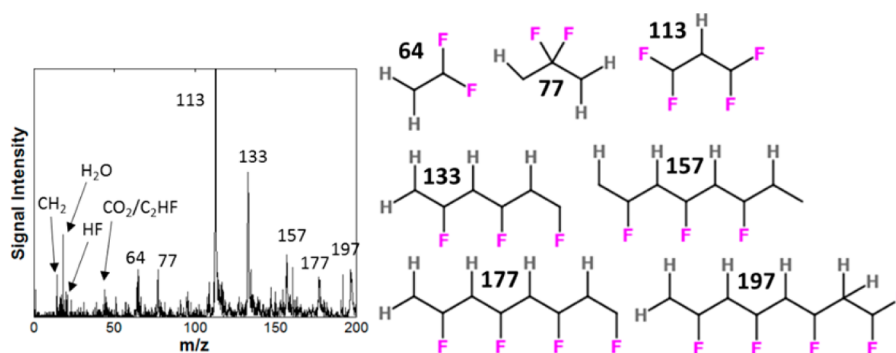


Figure 4. MS at 1.6 ms ( $\sim 700$  °C) of PVDF film and likely fragments labeled in spectra.

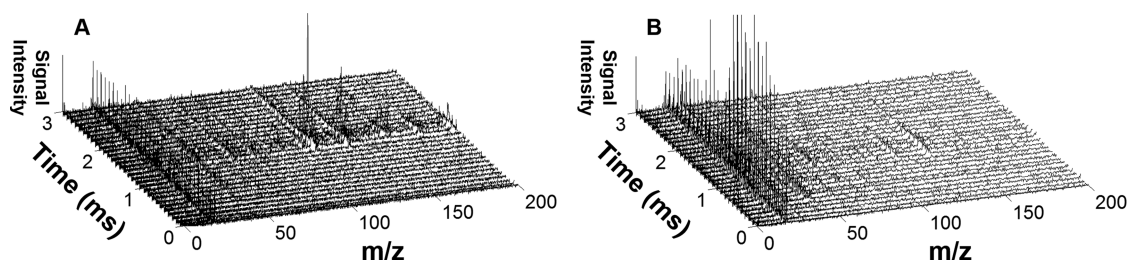


Figure 5. 3D plots of time-resolved spectra obtained from T-jump TOFMS of PVDF (A) and Al/PVDF (B) films.

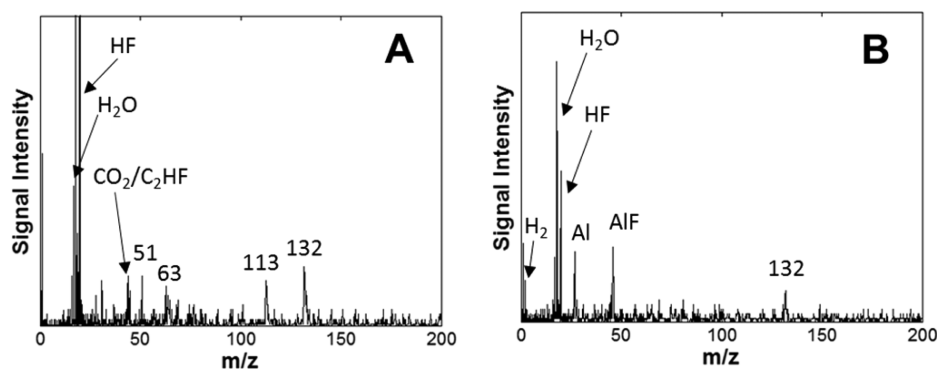


Figure 6. MS of Al/PVDF film at peak HF signal intensity (A: 1.3 ms, 600 °C) and peak AlF signal intensity (B: 1.8 ms, 780 °C).

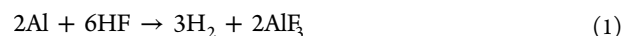
TOFMS allows for the collection of a full spectra every 0.1 ms allowing for higher heating rates consistent with combustion times.

Large masses ( $>50$   $m/z$ ) are observed, which are identified with likely species in Figure 4. The most striking feature is the small amount of HF, which is just the opposite to that observed at low heating rates.<sup>15</sup>

Figure 5 shows the time-resolved full spectra of the pure PVDF (A) and Al/PVDF (B). As seen in Figure 5, the PVDF decomposition products are detected earlier when nAl is present, corresponding to a decrease in the PVDF decomposition temperature.

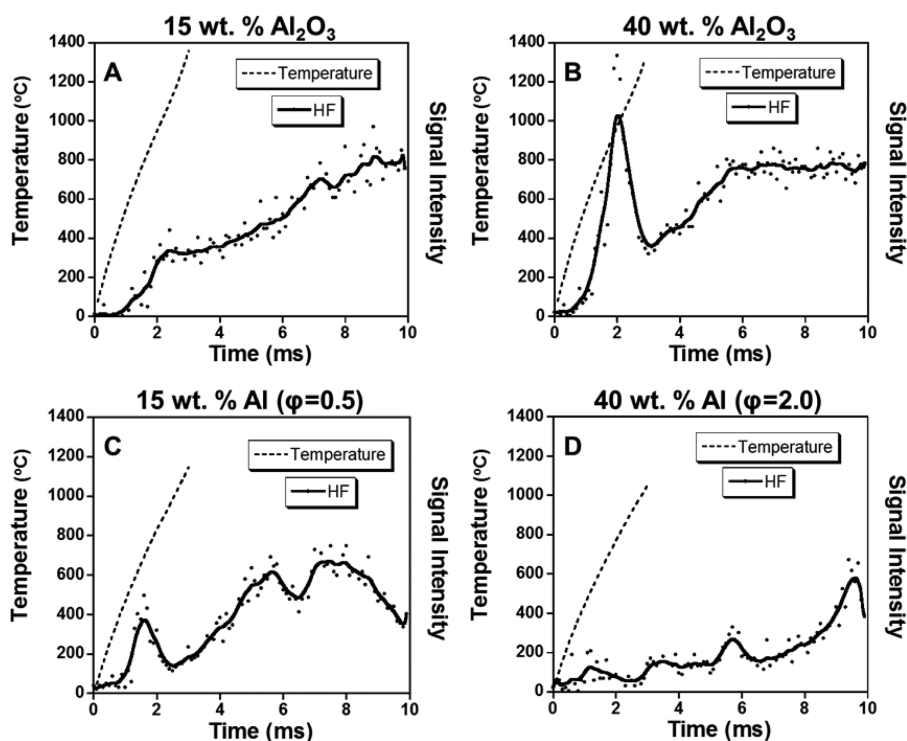
PVDF decomposition occurs at  $\sim 650$  °C in the pure PVDF film and at  $\sim 450$  °C in the Al/PVDF film. The temperature difference is about 200 °C at the high heating rate of the T-jump experiment ( $\sim 10^5$  K/s) while the temperature difference is only 100 °C in the previously published TGA/DSC experiments (20 °C/s).<sup>8</sup> Adding Al also significantly diminishes formation of large mass species, implying Al not only lowers the decomposition temperature but also promotes a more complete decomposition of the polymer.

Figure 6 shows detected species at the peak HF (A: 1.3 ms; 600 °C) and peak AlF (B: 1.8 ms, 780 °C) signal intensities. HF was detected prior to any AlF-containing gas phase species, consistent with nAl being oxidized by the gas phase PVDF decomposition product, HF. The nAl fluorination reaction would proceed as follows:



The evolution of  $\text{H}_2$  gas in the MS is observed concurrently with detection of AlF as seen in Figure 6B. It is also important to note that the larger mass decomposition products vary slightly from the pure PVDF film. Fragments of  $m/z = 132$  and 63 are observed, which are 1  $m/z$  lower than the described 133 and 64 peaks above. This correlates to the loss of a hydrogen from these fragments, resulting from more HF production in the Al/PVDF case.

The PIR between the  $\text{Al}_2\text{O}_3$  shell of the Al and condensed phase F-containing species is suspected to be the cause of the altered PVDF decomposition as the  $\text{Al}_2\text{O}_3$  creates a boundary between Al and PVDF and the Al is unable to diffuse through the shell in the decomposition temperature range. The catalyzed PVDF decomposition begins at  $\sim 450$  °C while the



**Figure 7.** Temporal wire temperature and HF signal intensity for 15 wt % Al<sub>2</sub>O<sub>3</sub> (A), 40 wt % Al<sub>2</sub>O<sub>3</sub> (B), fuel-lean 15 wt % Al (C), and fuel-rich 40 wt % Al (D) containing PVDF films. Absolute signal intensity scale and approximate amount of film on the wire are consistent for (A–D).

melting point of Al is not until 660 °C. While some may argue Al<sub>2</sub>O<sub>3</sub> is acting as a coreactant, in this context, the PVDF decomposition is said to be catalyzed simply because Al<sub>2</sub>O<sub>3</sub> remains unchanged, as diagnosed by XRD, at the end of the process. This reaction promotes a lower temperature decomposition and increased HF generation from PVDF as seen in Figures 5 and 6. In order to isolate the role of Al<sub>2</sub>O<sub>3</sub> in the reaction mechanism with PVDF, films were created containing 50 nm Al<sub>2</sub>O<sub>3</sub> particles in a PVDF matrix. Films of varying Al<sub>2</sub>O<sub>3</sub>/PVDF ratios were electrospayed onto Pt wires for T-jump TOFMS. The mass of PVDF used in the precursor solution was kept constant for this particular study.

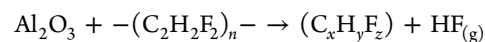
Figure 7A–D shows temporal HF and temperature profiles for alumina- and Al-containing films. For the Al case, 15 and 40 wt % correspond to Al/PVDF equivalence ratios of 0.5 and 2, respectively. Increasing the alumina content results in both an earlier onset (~450 °C) of HF appearance as well as an increase. At higher temperatures HF evolution increases and does so well past the termination of heating. It is also important to note that these experiments are done in a vacuum where the lack of heat transfer from the platinum filament to the surrounding atmosphere allows the wire to stay hot, well after the heating pulse is completed. The first HF increase is attributed to decomposition of PVDF catalyzed by the condensed phase PIR with Al<sub>2</sub>O<sub>3</sub>. We propose that the PIR results in the creation of condensed phase fluorinated Al<sub>2</sub>O<sub>3</sub> products along with some leftover condensed phase C<sub>x</sub>H<sub>y</sub>F<sub>z</sub> species that presumably further decompose to account for the second stage of HF release. XRD analysis of Al<sub>2</sub>O<sub>3</sub>/PVDF films that were heated in an argon environment at 1000 °C for 2 h showed only the Al<sub>2</sub>O<sub>3</sub> starting material (same phase) and no AlOF species (Figure S4). This implies that any surface reaction may lead to an amorphous fluorine-containing product. Sarbak et al. have also seen a similar result of no

new peaks corresponding to new F-containing species on fluorinated  $\gamma$ -phase Al<sub>2</sub>O<sub>3</sub>.<sup>16</sup> It is also likely that the AlOF species formed on the surface of the Al<sub>2</sub>O<sub>3</sub> decompose during further heating after the PIR occurs. The decomposition of AlOF species may also contribute to the second stage of HF release observed in Figure 7A,B.

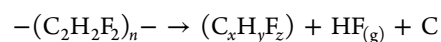
When using Al rather than alumina, a sharp HF peak is observed for the fuel lean sample (Figure 7C) (15 wt % corresponding to an equivalence ratio,  $\phi$ , of 0.5), but the peak intensity is diminished and shifts to a later time for fuel-rich samples (Figure 7D). The equivalence ratio was determined taking into account the 81% active Al content of the Al nanoparticles used. The initial high intensity HF release is presumably due to the rapid decomposition of PVDF, which is catalyzed by the PIR between the Al<sub>2</sub>O<sub>3</sub> shell of the Al and the fluorine of the PVDF. When there are large amounts of Al in the film, the early stage HF is subsequently rapidly consumed in the fluorination of Al, resulting in the creation of the final reaction product, AlF<sub>3</sub>.

The PIR facilitates a rapid release of HF that reacts with Al, leading to the creation of AlF species and hydrogen. The following reactions seen in Figure 8 outline this process with step A occurring first at ~450 °C and steps B, C, and D occurring in parallel:

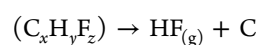
(A) catalyzed PVDF decomposition (PIR)



(B) direct pyrolysis of PVDF



(C) decomposition of intermediates



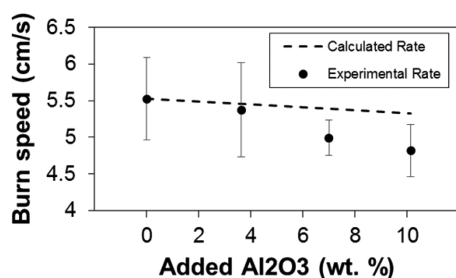
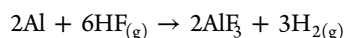


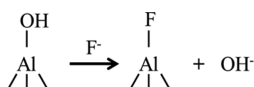
**Figure 8.** Burn speeds for stoichiometric Al/PVDF films with varying amounts of added Al<sub>2</sub>O<sub>3</sub>.

(D) fluorination of aluminum



HF generation is possible through three different reactions. Reaction A shows the catalyzed PVDF decomposition resulting in the rapid low temperature release of HF. As the Al<sub>2</sub>O<sub>3</sub> concentration is increased (Figure 7B), more of the PVDF can react with the Al<sub>2</sub>O<sub>3</sub> as seen by the increase in the first stage of HF release in comparison to the lower concentration case (Figure 7A). PVDF that is not in direct contact with Al<sub>2</sub>O<sub>3</sub> can pyrolyze to form C<sub>x</sub>H<sub>y</sub>F<sub>z</sub> species, HF, and carbon (reaction B). The remaining C<sub>x</sub>H<sub>y</sub>F<sub>z</sub> species (reaction C) continue to decompose, releasing even more HF over a prolonged period of time. The decomposition of C<sub>x</sub>H<sub>y</sub>F<sub>z</sub> species and pyrolysis of PVDF are proposed to be much slower processes as the secondary HF release peaks in Figure 7 are much broader than the low temperature HF release from the Al<sub>2</sub>O<sub>3</sub>-catalyzed decomposition. Fluorination of Al (reaction D) occurs once HF available, and either the Al core is exposed by the fluorination of its Al<sub>2</sub>O<sub>3</sub> shell or the Al has diffused outward as has been demonstrated in previous reports.<sup>17,18</sup>

**Al/PVDF Reaction Mechanism Summary.** The above results show the importance of the nascent oxide shell on the aluminum nanoparticles to the Al/PVDF reaction occurring in the nanocomposite thin films. Before aluminum oxidation can occur, the Al<sub>2</sub>O<sub>3</sub> + PVDF PIR forms Al<sub>x</sub>O<sub>y</sub>F<sub>z</sub> species while also rapidly producing HF<sub>(g)</sub> through the decomposition of C<sub>x</sub>H<sub>y</sub>F<sub>z</sub> species. This early stage HF<sub>(g)</sub> release should be limited by the available reaction sites on the surface of the Al<sub>2</sub>O<sub>3</sub>. This is demonstrated by the increase in relative HF signal intensity with an increase of Al<sub>2</sub>O<sub>3</sub> shown in Figure 7. The unstable Al<sub>x</sub>O<sub>y</sub>F<sub>z</sub> species formed during the PIR decompose with further heating, resulting in the second, prolonged stage of HF release observed in the temporal plots in Figure 7. T-jump TOFMS analysis in Figure 6 also showed the release of H<sub>2</sub>O<sub>(g)</sub> from the surface of the Al<sub>2</sub>O<sub>3</sub> that precedes any HF<sub>(g)</sub> generation. Sarbak has proposed that fluorine can form bonds with the surface of Al<sub>2</sub>O<sub>3</sub> that are facilitated through OH groups on the surface of Al<sub>2</sub>O<sub>3</sub><sup>16</sup> as follows:



In the case of the condensed phase PIR between Al<sub>2</sub>O<sub>3</sub> and PVDF, H<sub>2</sub>O must leave the surface sites in order for F to bind.

Any substantial changes to the alumina shell, as for example creation of the Al<sub>x</sub>O<sub>y</sub>F<sub>z</sub> species, will only increase to enhance the transport of elemental Al from the core to react with HF<sub>(g)</sub> producing AlF<sub>3</sub> and H<sub>2</sub>. Unstable Al<sub>x</sub>O<sub>y</sub>F<sub>z</sub> species can go on to decompose, along with any residual condensed phase fluorine-

containing PVDF decomposition products, resulting in the secondary prolonged release of HF that is observed in the TOFMS results.

**Burn Speed Analysis.** The results in Figure 7 show that the amount of Al<sub>2</sub>O<sub>3</sub> in the system directly correlates to the amount of early stage HF that is released. In order to test the effect of an enhanced PIR between Al<sub>2</sub>O<sub>3</sub> and PVDF on any macroscopic observable, Al<sub>2</sub>O<sub>3</sub> was added to the precursor solution for stoichiometric Al/PVDF films in varying quantities and burn speeds were measured under 1 atm of argon. As shown in Figure 8, the addition of Al<sub>2</sub>O<sub>3</sub> resulted in a decrease in burn speed when compared to the stoichiometric Al/PVDF film (0 wt % of added Al<sub>2</sub>O<sub>3</sub>), signifying that although Al<sub>2</sub>O<sub>3</sub> promotes the low temperature release of HF, this does not translate into any enhancement in global combustion rate.

Four possible causes of such a decrease in burn speed caused by the addition of Al<sub>2</sub>O<sub>3</sub> include (i) Al<sub>2</sub>O<sub>3</sub> acting as a diluent, thus decreasing the energy available for propagation, (ii) Al<sub>2</sub>O<sub>3</sub> catalyzes the release of oxidizing species faster than Al can react with these species, (iii) the creation of condensed phase Al<sub>x</sub>O<sub>y</sub>F<sub>z</sub> species by direct reaction of Al<sub>2</sub>O<sub>3</sub> with PVDF, and/or (iv) a morphological change in the film altering the interfacial contact area between Al and PVDF.

In order to estimate the isolated effect of Al<sub>2</sub>O<sub>3</sub> acting as a heat sink during the reaction of Al and PVDF, the ratio of reaction rates of a pure Al/PVDF stoichiometric film, *R*, and an Al<sub>2</sub>O<sub>3</sub>-containing film, *R*<sub>Al<sub>2</sub>O<sub>3</sub></sub>, was approximated to be equivalent to the respective burn speed ratio, *v*<sub>exp</sub>/*v*<sub>calc</sub>, where *v*<sub>exp</sub> is the experimentally determined burn speed for the pure Al/PVDF film and *v*<sub>calc</sub> is the theoretical burn speed for a film with an added amount of Al<sub>2</sub>O<sub>3</sub>. We further assume that, all things being equal, if this is just a dilution effect, then the burn speeds should scale as the effective heat of reaction as shown in eq 2.

$$\frac{R}{R_{\text{Al}_2\text{O}_3}} = \frac{\Delta H_{\text{rxn}}}{\Delta H_{\text{rxn}}(1 - \chi_{\text{Al}_2\text{O}_3}) + (C_p \Delta T)_{\text{Al}_2\text{O}_3}(\chi_{\text{Al}_2\text{O}_3})} \approx \frac{v_{\text{exp}}}{v_{\text{calc}}} \quad (2)$$

The calculated burn speed shown in Figure 8 corresponds to *v*<sub>calc</sub> in the following equation for the respective amount of added Al<sub>2</sub>O<sub>3</sub>. The enthalpy of reaction for the stoichiometric Al/PVDF film with no additional Al<sub>2</sub>O<sub>3</sub>, Δ*H*<sub>rxn</sub> (kJ/mol), was calculated for the fluorination of Al by HF, which can be seen in reaction D. (*C*<sub>p</sub>Δ*T*)<sub>Al<sub>2</sub>O<sub>3</sub></sub> represents the energy required to heat the added Al<sub>2</sub>O<sub>3</sub> from room temperature to the experimental ignition temperature at 1 atm of argon (~825 °C as shown in Figure 2). Heats of formation for HF and AlF<sub>3</sub> of −273.2 and −1209 kJ/mol, respectively, and a (*C*<sub>p</sub>Δ*T*)<sub>Al<sub>2</sub>O<sub>3</sub></sub> of 90.5 kJ/mol were obtained from the NIST WebBook. The theoretical amount of HF generated from the complete decomposition of the PVDF in the film is taken into account when calculating the mole fraction of Al<sub>2</sub>O<sub>3</sub>, χ<sub>Al<sub>2</sub>O<sub>3</sub></sub>. The reaction rates in eq 2 are equal to the enthalpy of reaction divided by a characteristic time. Evident from the calculated curve plotted in Figure 8, the heat absorbing effect of Al<sub>2</sub>O<sub>3</sub> is only partially responsible for the experimental decrease in burn speed.

The second potential explanation for the decrease in burn speed is Al<sub>2</sub>O<sub>3</sub> catalyzing the PVDF decomposition before the Al is ready to react with the gas phase HF being generated. This situation is highly unlikely because the T-jump TOFMS results in Figure 7C,D show a decrease in early onset HF signal

intensity for fuel-rich samples. If the Al was unable to react during the early onset HF release, the preliminary HF signal intensity would be consistent among fuel-rich (Figure 7D) and fuel-lean (Figure 7C) samples. Figure 7A,B also shows that increasing the amount of Al<sub>2</sub>O<sub>3</sub> in a PVDF film will increase the amount of early onset HF generated but does not alter the temperature in which the catalyzed decomposition occurs.

The third potential effect that added Al<sub>2</sub>O<sub>3</sub> may have is that, in addition to catalyzing the decomposition, the Al<sub>2</sub>O<sub>3</sub> is reacting with the PVDF and/or PVDF decomposition products to form Al<sub>x</sub>O<sub>y</sub>F<sub>z</sub> species, thusly decreasing the amount of reactive fluorine to fluorinate the Al. XRD analysis of Al<sub>2</sub>O<sub>3</sub>/PVDF films after heating (Figure S4) does not show any crystalline Al<sub>x</sub>O<sub>y</sub>F<sub>z</sub> species, and the TGA results in Figure 3B show a final mass that is identical to the initial mass of pure Al<sub>2</sub>O<sub>3</sub> in the film. Both of these results show that while the Al<sub>2</sub>O<sub>3</sub> has a catalytic effect on the decomposition of PVDF, it does not decrease the amount of reactive fluorine species available to fluorinate the Al.

The final, and what we consider to be an additional, most likely explanation for the burn speed reduction is the change in interfacial area between Al and PVDF with the addition of Al<sub>2</sub>O<sub>3</sub>. Adding Al<sub>2</sub>O<sub>3</sub> hinders the fluorination of aluminum by acting as a storage mechanism for fluorine. This is an interfacial area explanation, and if the conjecture is correct, then there may be advantages of to making laminates composed of Al/PVDF and Al<sub>2</sub>O<sub>3</sub>/PVDF bilayers. We are in the process of exploring this possibility.

## CONCLUSION

The PIR between Al<sub>2</sub>O<sub>3</sub> and PTFE has been previously identified as a key initiating step in the reaction between aluminum and the fluoropolymer. This PIR was recently identified as a key component in the Al/PVDF reaction—a system that has gained attention due to the ease of processing and ability to create films with high mass loadings of nanosized constituents using electrospray deposition methods.<sup>8</sup> Using T-jump ignition in different environments, it was determined that the Al in the Al/PVDF system does not react in the condensed phase and is oxidized by gaseous HF released as a decomposition product of PVDF. TGA/DSC analysis showed an exothermic decomposition for PVDF film in the presence of oxygen and also clearly showed a low temperature PIR when Al<sub>2</sub>O<sub>3</sub> was incorporated into the film. These experiments also showed a clear increase in heat release for the PIR and PVDF decomposition with an increase in heating rate, further supporting the need for high heating rate analytics to be performed.

The Al/PVDF reaction mechanism was further probed using T-jump TOFMS and the condensed phase PIR between PVDF and the Al<sub>2</sub>O<sub>3</sub> shell of the nAl caused the PVDF to decompose more completely and at a lower temperature. This more complete decomposition promotes the generation of gas phase HF that can go on to oxidize the Al. Al<sub>2</sub>O<sub>3</sub> was added to Al/PVDF films to see if increasing the amount of low temperature HF generated would have an effect on the burn speed of a thin film. No burn speed enhancements were observed, and it was concluded that adding Al<sub>2</sub>O<sub>3</sub> to the system hinders the Al/PVDF reaction propagation in the film. Future work will entail using these results to create multilayer films containing Al, Al<sub>2</sub>O<sub>3</sub>, and PVDF that can maintain the desired Al/PVDF interfacial area while also containing thin layers of Al<sub>2</sub>O<sub>3</sub>/PVDF that can rapidly supply the Al with reactive HF. Further

understanding of the Al/PVDF reaction mechanism is essential to the understanding of multilayered laminates based off of the Al/PVDF system and multicomponent thermite systems such as Al/CuO/PVDF.

## ASSOCIATED CONTENT

### Supporting Information

The Supporting Information is available free of charge on the ACS Publications website at DOI: 10.1021/acs.jpcc.6b01100.

Images from high speed video of Al/PVDF ignition in different environments; XRD of Al<sub>2</sub>O<sub>3</sub>/PVDF films before and after heating (PDF)

## AUTHOR INFORMATION

### Corresponding Author

\*E-mail [mrz@umd.edu](mailto:mrz@umd.edu); Ph 301-405-4311 (M.R.Z.).

### Notes

The authors declare no competing financial interest.

## ACKNOWLEDGMENTS

This work was supported by the Army Research Office and the Defense Threat Reduction Agency. We acknowledge the support of the UMD X-ray Crystallographic Center for help with the XRD analysis. We also acknowledge the support of the Maryland Nanocenter and its AIMLab. The AIMLab is supported in part by the NSF as a MRSEC Shared Experimental Facility.

## REFERENCES

- (1) Pivkina, A.; Ulyanova, P.; Frolov, Y.; Zavyalov, S.; Schoonman, J. Nanomaterials for Heterogeneous Combustion. *Propellants, Explos., Pyrotech.* **2004**, *29*, 39–48.
- (2) Dreizin, E. L. Metal-Based Reactive Nanomaterials. *Prog. Energy Combust. Sci.* **2009**, *35*, 141–167.
- (3) Cohen, N. S.; Fleming, R. W.; Derr, R. L. Role of Binders in Solid-Propellant Combustion. *AIAA J.* **1974**, *12*, 212–218.
- (4) Kubota, N.; Serizawa, C. Combustion Process of Magnesium/Polytetrafluoroethylene Pyrotechnics. *Propellants, Explos., Pyrotech.* **1987**, *12*, 145–8.
- (5) Koch, E.-C. Metal-fluorocarbon-pyrolants: III. Development and Application of Magnesium/Teflon/Viton (MTV). *Propellants, Explos., Pyrotech.* **2002**, *27*, 262–266.
- (6) Osborne, D. T.; Pantoya, M. L. Effect of Al Particle Size on the Thermal Degradation of Al/Teflon Mixtures. *Combust. Sci. Technol.* **2007**, *179*, 1467–1480.
- (7) Pantoya, M. L.; Dean, S. W. The Influence of Alumina Passivation on Nano-Al/Teflon Reactions. *Thermochim. Acta* **2009**, *493*, 109–110.
- (8) Huang, C.; Jian, G.; DeLisio, J. B.; Wang, H.; Zachariah, M. R. Electrospray Deposition of Energetic Polymer Nanocomposites with High Mass Particle Loadings: A Prelude to 3D Printing of Rocket Motors. *Adv. Eng. Mater.* **2015**, *17*, 95–101.
- (9) Li, X.; Guerieri, P.; Zhou, W.; Huang, C.; Zachariah Michael, R. Direct Deposit Laminate Nanocomposites with Enhanced Propellant Properties. *ACS Appl. Mater. Interfaces* **2015**, *7*, 9103–9.
- (10) McCollum, J.; Pantoya, M. L.; Iacono, S. T. Activating Aluminum Reactivity with Fluoropolymer Coatings for Improved Energetic Composite Combustion. *ACS Appl. Mater. Interfaces* **2015**, *7*, 18742–18749.
- (11) Mulamba, O.; Pantoya, M. Exothermic Surface Reactions in Alumina-Aluminum Shell-Core Nanoparticles with Iodine Oxide Decomposition Fragments. *J. Nanopart. Res.* **2014**, *16*, 2310-1–2310-9.
- (12) Hobosyan, M. A.; Kirakosyan, K. G.; Kharatyan, S. L.; Martirosyan, K. S. PTFE-Al<sub>2</sub>O<sub>3</sub> Reactive Interaction at High Heating Rates. *J. Therm. Anal. Calorim.* **2015**, *119*, 245–251.

- (13) Zhou, L.; Piekiet, N.; Chowdhury, S.; Zachariah, M. R. T-Jump/Time-of-Flight Mass Spectrometry for Time-Resolved Analysis of Energetic Materials. *Rapid Commun. Mass Spectrom.* **2009**, *23*, 194–202.
- (14) Mulamba, O.; Pantoya, M. L. Exothermic Surface Chemistry on Aluminum Particles Promoting Reactivity. *Appl. Surf. Sci.* **2014**, *315*, 90–94.
- (15) Zulfqar, S.; Zulfqar, M.; Rizvi, M.; Munir, A.; McNeill, I. C. Study of the Thermal Degradation of Poly(chlorotrifluoroethylene), Poly(vinylidene Fluoride) and Copolymers of Chlorotrifluoroethylene and Vinylidene Fluoride. *Polym. Degrad. Stab.* **1994**, *43*, 423–30.
- (16) Sarbak, Z. Effect of Fluoride and Sodium Ions on Structural and Thermal Properties of Gamma-Al<sub>2</sub>O<sub>3</sub>. *Cryst. Res. Technol.* **1997**, *32*, 491–497.
- (17) Zhang, S.; Dreizin, E. L. Reaction Interface for Heterogeneous Oxidation of Aluminum Powders. *J. Phys. Chem. C* **2013**, *117*, 14025–14031.
- (18) Rai, A.; Park, K.; Zhou, L.; Zachariah, M. R. Understanding the Mechanism of Aluminium Nanoparticle Oxidation. *Combust. Theory Modell.* **2006**, *10*, 843–859.